

UCAN: Unified Convolutional Attention Network for Expansive Receptive Fields in Lightweight Super-Resolution

Cao Thien Tan^{1,2,3} Trang Phan Thi Thu^{3,5} Duc Nghiem Do⁶ Ho Ngoc Anh⁵
 Hanyang Zhuang^{4,*} Duc Dung Nguyen^{2,*}

¹Ho Chi Minh City Open University ²AI Tech Lab, Ho Chi Minh City University of Technology

³Code Mely AI Research Team ⁴Global College, Shanghai Jiao Tong University

⁵Ha Noi University of Science and Technology ⁶University of Manitoba

caothientan2001@gmail.com, zhuanghany11@sjtu.edu.cn, nddung@hcmut.edu.vn

Code: <https://github.com/hokiyoshi/UCAN>

Abstract

Hybrid CNN-Transformer architectures achieve strong results in image super-resolution, but scaling attention windows or convolution kernels significantly increases computational cost, limiting deployment on resource-constrained devices. We present UCAN, a lightweight network that unifies convolution and attention to expand the effective receptive field efficiently. UCAN combines window-based spatial attention with a Hedgehog Attention mechanism to model both local texture and long-range dependencies, and introduces a distillation-based large-kernel module to preserve high-frequency structure without heavy computation. In addition, we employ cross-layer parameter sharing to further reduce complexity. On Manga109 (4 \times), UCAN-L achieves 31.63 dB PSNR with only 48.4G MACs, surpassing recent lightweight models. On BSDS100, UCAN attains 27.79 dB, outperforming methods with significantly larger models. Extensive experiments show that UCAN achieves a superior trade-off between accuracy, efficiency, and scalability, making it well-suited for practical high-resolution image restoration.

1. Introduction

Single-image super resolution (SR) aims to reconstruct high resolution (HR) images from degraded low resolution (LR) inputs, representing a long-standing yet continually evolving challenge in low-level vision. This task has garnered sustained attention in the computer vision community, driven by its broad spectrum of practical applications and the increasing demand for both accuracy and efficiency in SR solutions. Recent advancements have seen the emergence of

*Corresponding author

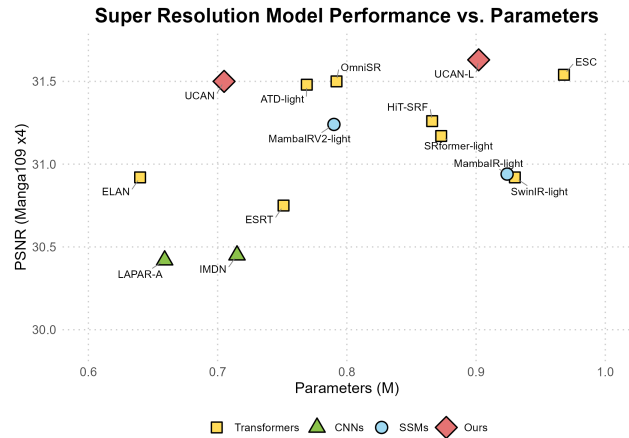


Figure 1. Performance comparison of PSNR versus model parameters on the Manga109 ($\times 4$) dataset. Our method is evaluated alongside state-of-the-art super-resolution approaches. Green triangles represent CNN-based methods, yellow squares denote Transformer-based methods, blue circles indicate SSM-based methods, and red diamonds show our proposed approach.

lightweight SR models, with growing emphasis on enhancing performance by expanding the effective receptive field. While transformer-based architectures have demonstrated strong capability in this regard, recent research investigates alternative strategies that extend the receptive field through new architectures or techniques with lower computational complexity and fewer parameters.

Recent advances in lightweight super-resolution primarily focus on enlarging the effective receptive field to capture broader contextual information and recover high-frequency details. While this expansion is essential, existing approaches remain limited. Convolution-based architectures

effectively model local dependencies, yet many efforts to introduce global attention such as Grid Attention [33], Mamba [8, 29], and Adaptive Token Dictionary [38] still struggle with inefficiency in capturing global context. Linear attention [1] offers a promising alternative, but its potential is constrained by limited feature diversity, which weakens representational capacity. Moreover, the trade-off between efficiency and performance persists; although recent models achieve lower parameter counts, they often sacrifice representational richness. Joint attention mechanisms and distillation strategies [26] further homogenize feature maps across layers and channels, reducing feature diversity and ultimately hindering reconstruction quality.

We introduce the Unified Convolutional Attention Network (UCAN), a lightweight super-resolution architecture that expands the effective receptive field while preserving rich feature representation. The High Performance Block incorporates Flash Attention to avoid computing the full attention matrix, allowing an efficient 32×32 window and achieving substantially lower latency compared to conventional attention. To capture fine local structures, long-range dependencies, and channel relationships, we design a Hybrid Attention mechanism where windowed attention efficiently models local patterns, and the Dual Fusion Layer, an optimized implementation of Hedgehog Attention, addresses the rank deficiency typically observed in linear and channel attention. In addition, parameter sharing is employed to reduce computational cost while maintaining strong performance. A Large Kernel Distillation module further enhances the network’s ability to reproduce complex textures and hierarchical structures with minimal parameter overhead. Across standard benchmarks, UCAN delivers higher visual fidelity while preserving a favorable balance between latency and computational efficiency.

Building upon the aforementioned components, UCAN demonstrates a strong balance between lightweight design and expressive capability. As shown in Fig. 1, UCAN achieves competitive performance with a favorable trade-off between parameter count and reconstruction accuracy. On standard benchmarks for $2\times$ upscaling, UCAN surpasses the OmniSR model by **0.12 dB** on Urban100 and **0.17 dB** on Set5, while using **11% fewer parameters** and **24% fewer FLOPs**. For $4\times$ upscaling on Manga109, the larger variant UCAN-L outperforms MambaIRV2 by **0.39 dB**, achieving up to **36% lower computational cost**. These consistent improvements highlight the effectiveness and efficiency of our unified convolutional attention framework in achieving high-fidelity image reconstruction.

In summary, our contributions are given as follows:

- We introduce Hedgehog Attention, a novel attention mechanism that enhances feature diversity in linear attention by enhancing the rank of features. This design allows the model to capture richer and more expressive features.

- We propose UCAN, a unified and efficient model that captures both local and global dependencies across multiple receptive fields. UCAN employs Flash Attention for large-window attention to improve computational efficiency, Hedgehog Attention to model global information with strong robustness under limited resources, and multi-kernel convolution to extract essential local features.
- We design a semi-sharing and distillation architecture that balances parameter sharing with task-specific specialization. Experimental results show that this architecture allows UCAN to achieve strong performance while substantially reducing the number of parameters and computational cost.

2. Related work

Convolutional Methods. Early deep learning-based SR methods [4, 5] employed stacked convolutions for local feature extraction but suffered from over-parameterization. Weight-sharing strategies [13, 14, 32] reduced complexity, yet input-independent sharing often degraded performance. Later architectures improved CNN expressiveness: EDSR [20] with deep residual blocks, RDN [43] with dense feature reuse, and RCAN [42] with channel attention. Despite these advances, convolutions remain constrained to local receptive fields, motivating the exploration of architectures that model long-range dependencies.

Comparative Analysis of Attention Methods. Vision Transformers have recently gained traction in image super-resolution following their success in general computer vision tasks [6, 27]. Representative methods include SwinIR [22], which adapts the shifted-window strategy for image restoration, ESRT [23], which combines lightweight CNNs with transformer blocks for efficiency, and ELAN [40], which reduces cost through shared self-attention and unified query-key parameters [36].

Despite these advances, contemporary transformer architectures still suffer from limited effective receptive fields, restricting global context modeling and computational efficiency. To address this, Omni-SR [33] introduced grid attention to enlarge spatial observation, while MambaIRv2 [8] combined Swin Transformer with State Space Models to enhance whole-image information capture. Building on these ideas, our approach integrates Swin Transformer with an improved Linear Transformer, achieving superior performance by extending the receptive field while remaining efficient.

Large Receptive Field Attention Mechanisms. The computational cost of Transformers has driven research into CNN-based alternatives that use large kernels and pixel-level attention to approximate Transformer performance [30, 34, 35]. However, these methods often fail to capture self-attention’s rich representations or incur memory overhead from complex architectures like multi-directional

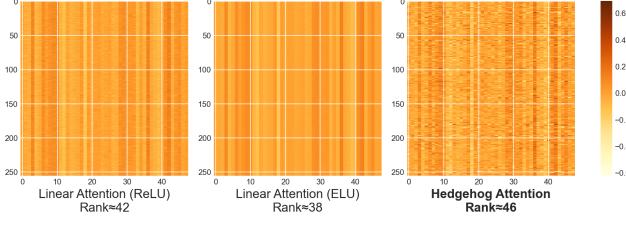


Figure 2. Comparison of feature maps output by Linear Attention (Using ReLU, ELU feature maps) and Hedgehog Attention. All experiments are conducted based on an image with $N = 256$ and $d = 48$. The full rank of matrices in the figure is 64. This figure shows that our model outperforms previous methods in diversity.

scanning. Recent work has addressed CNN kernel expansion through CUDA optimization [16], asymmetric convolutions [31], dilated convolutions [16], and distillation techniques [17]. Building on these advances, we propose Large Kernel Distillation, which combines dilated convolutions with knowledge distillation to achieve large receptive fields while maintaining computational efficiency.

3. Proposed Method

In this section, we begin with an analysis of Linear Transformers and Softmax Attention, and then provide a detailed description of the proposed network.

3.1. Bridging Softmax and Linear Attention

Connection Analysis. Let $\mathbf{X} \in \mathbb{R}^{HW \times C}$ and $\mathbf{Q} = \mathbf{X}\mathbf{W}_Q$, $\mathbf{K} = \mathbf{X}\mathbf{W}_K$, $\mathbf{V} = \mathbf{X}\mathbf{W}_V$ with $\mathbf{W}_Q, \mathbf{W}_K, \mathbf{W}_V \in \mathbb{R}^{C \times d}$. Denote rows by $\mathbf{q}_i, \mathbf{k}_i, \mathbf{v}_i \in \mathbb{R}^d$. Standard softmax attention is described as

$$\mathbf{s}_i = \left[\frac{\exp(\mathbf{q}_i^\top \mathbf{k}_1)}{\sum_{j=1}^N \exp(\mathbf{q}_i^\top \mathbf{k}_j)}, \dots, \frac{\exp(\mathbf{q}_i^\top \mathbf{k}_{HW})}{\sum_{j=1}^N \exp(\mathbf{q}_i^\top \mathbf{k}_j)} \right]^\top, \quad (1)$$

$$\mathbf{o}_i^S = \mathbf{s}_i^\top \mathbf{V}.$$

However, linear attention substitutes $\exp(\mathbf{q}_i^\top \mathbf{k}_j)$ by $\phi(\mathbf{q}_i)^\top \phi(\mathbf{k}_j)$ for a feature map $\phi \in \mathbb{R}^d \rightarrow \mathbb{R}^r$

$$\mathbf{o}_i^L = \frac{\sum_{j=1}^N (\phi(\mathbf{q}_i)^\top \phi(\mathbf{k}_j)) \mathbf{v}_j}{\sum_{j=1}^N \phi(\mathbf{q}_i)^\top \phi(\mathbf{k}_j)} = \frac{\phi(\mathbf{q}_i)^\top (\sum_{j=1}^N \phi(\mathbf{k}_j) \mathbf{v}_j^\top)}{\phi(\mathbf{q}_i)^\top (\sum_{j=1}^N \phi(\mathbf{k}_j))}. \quad (2)$$

The two aggregated terms $\sum_j \phi(\mathbf{k}_j) \mathbf{v}_j^\top$ and $\sum_j \phi(\mathbf{k}_j)$ are computable in $\mathcal{O}(N)$ and reused for all queries, reducing per layer complexity from $\mathcal{O}(N^2)$ to $\mathcal{O}(N)$.

Breaking the low rank bottleneck in linear attention.

Previous work restores the rank of the output matrix by adding depthwise convolutions or auxiliary high rank multipliers, but this does not remove the intrinsic low rank tendency of linear attention. Rank collapse forces the model to

rely on a few dependent directions and reduces representational diversity.

Approximating softmax in linear time requires a feature map ϕ that reproduces softmax selectivity. Simple choices such as ReLU or ELU+1 fail since ReLU discards negative contributions that can combine to form important positive attention under softmax, while ELU+1 yields extreme relative variations that encourage rank collapse. A detailed analysis appears in the supplementary material.

We use the Hedgehog Feature Map (HFM) [39]. HFM concatenates m symmetric exponential feature pairs

$$\phi_H(\mathbf{X}) = [\exp(\mathbf{W}^\top \mathbf{X} + \mathbf{b}_1), \dots, \exp(\mathbf{W}^\top \mathbf{X} + \mathbf{b}_m), \exp(-\mathbf{W}^\top \mathbf{X} - \mathbf{b}_1), \dots, \exp(-\mathbf{W}^\top \mathbf{X} - \mathbf{b}_m)], \quad (3)$$

where $\mathbf{W} \in \mathbb{R}^{C \times C}$ is a shared projection and $\{\mathbf{b}_i\}_{i=1}^m$ are learnable biases.

The HFM presents distinct advantages stemming from its core design. Its simple, trainable MLP style construction affords greater flexibility than rigid, hand designed feature maps. By promoting low entropy, spike like attention distributions, HFM also maintains fine grained, content dependent lookups while simultaneously increasing diversity. Moreover, its symmetric pairing mechanism preserves information from both positive and negative pre projection directions, thereby mitigating the information loss often caused by rectification. Consequently, HFM is able to suppress rank collapse directly, eliminating the need for external rank recovery modules. Our experimental results in Fig. 2 show that the Linear Attention model applying HFM recovers a rank up to 46, exceeding other compared methods.

3.2. Overall architecture

We tackle the classic trade off between receptive field size and efficiency with a layered design that follows prior work [8, 17, 26, 38]. First, we build an efficient attention backbone that yields large receptive fields at low cost. On top of this backbone we stack hybrid blocks that integrate local detail and global context, and finally we distill spatial knowledge from large kernel blocks into the network so the model better preserves fine structures and intricate details.

A low resolution input image $\mathbf{I}_{LR} \in \mathbb{R}^{H \times W \times 3}$ is first mapped to shallow feature embeddings \mathbf{F}_0 by a 3×3 convolution. These shallow features are processed by a core encoder composed of Broad Effective Receptive Field Group (BERFG) units, represented by f_{BERFG} , to produce deep features \mathbf{F}_{df} . To retain low frequency content, we fuse \mathbf{F}_{df} with \mathbf{F}_0 to obtain \mathbf{F}_{fuse} . The fused features then pass through a reconstruction module (a 3×3 convolution followed by pixel shuffle [28]) to yield the final high resolution image \mathbf{I}_{HR} . The core encoder relies on the Broad Effective Receptive Field Group. This group sequentially integrates High Performance Attention for local context, Shared and Receive

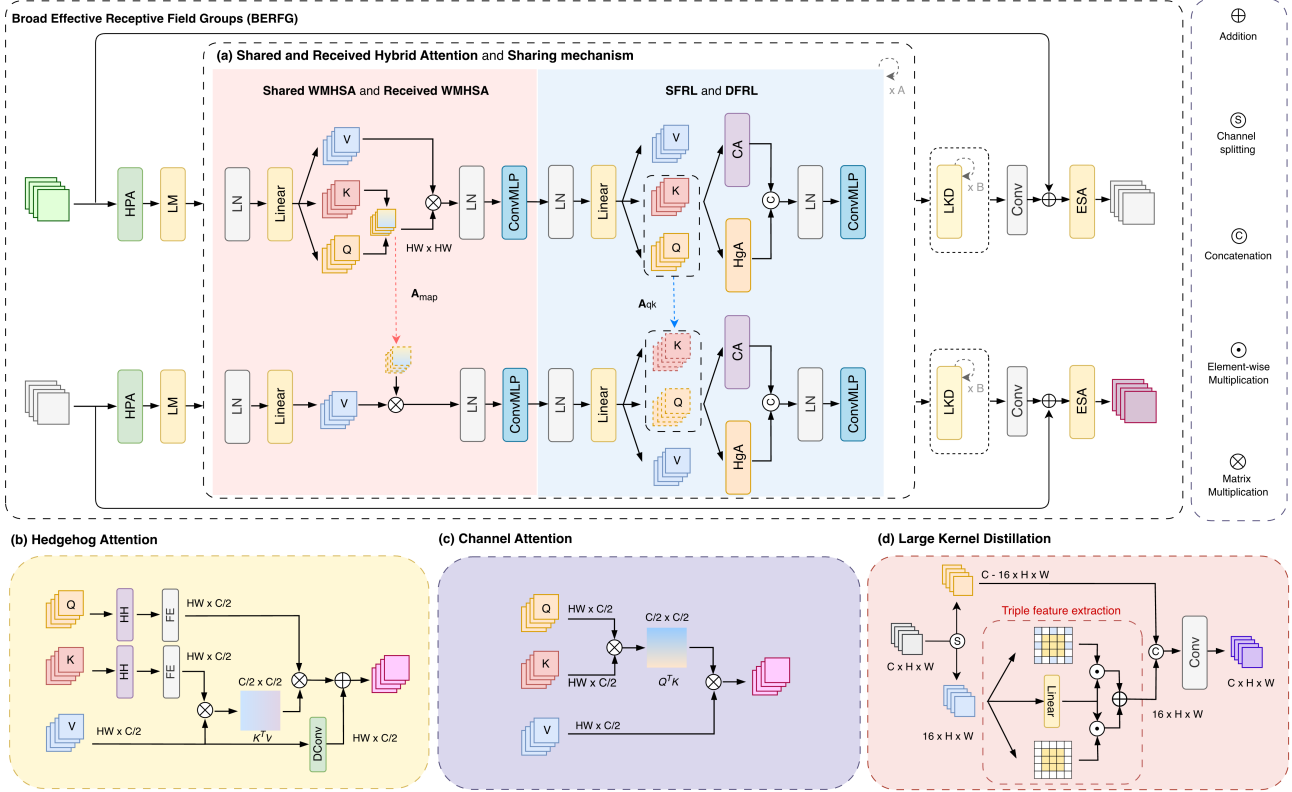


Figure 3. Detailed architecture of (a) Shared and Received Hybrid Attention (SHA and RHA) and (b) Large Kernel Distillation (LKD). LKD contains a Triple Feature Extraction block with three branches, which are the Large Kernel Spatial Branch, the Channel Branch, and the Small Kernel Spatial Branch. SHA and RHA employ Shared and Received Window Multi Head Self Attention (Shared WMHSA and Received WMHSA) to capture local information, and include a Shared Dual Fusion Layer (SDFL) and a Dual Fusion Receiver Layer (DFRL) to aggregate global context. The Dual Fusion Layer comprises two sub branches, which are Hedgehog Attention (HgA) and Channel Attention (CA).

Hybrid Attention for efficient global aggregation, and Large Kernel Distillation for spatial refinement. We detail these submodules in the following subsections.

3.3. Broad Effective Receptive Field Group

To optimize the computational cost of deep attention mechanisms, we propose the Broad Effective Receptive Field Group (BERFG), a two part architecture consisting of a Sharing Block (SB) and a Receiving Block (RB) (Fig. 3).

The Sharing Block first processes the input features, F_{in} , and passes them through an initial transformation using High Performance Attention (HPA) and Local Module (LM) layers [26]. The result then enters a series of Shared Hybrid Attention (f_{SHA}) modules that perform the full attention computation. As shown in the equation 4, these modules critically share $A_{qk}^{(a)}$ and $A_{map}^{(a)}$ as

$$F_{2,a+1}, A_{map}^{(a)}, A_{qk}^{(a)} = f_{SHA}^{(a)}(F_{2,a}) \quad (4)$$

The features are subsequently refined by Large Kernel Dis-

tillation (LKD) layers. Finally, the SB output, $F_{SB,out}$, is produced by an Enhanced Spatial Attention (ESA) module [21] applied after a residual connection with the initial input, F_{in} .

The Receiving Block takes $F_{SB,out}$ as its input and mirrors its structure. However, it introduces our core optimization within its Received Hybrid Attention (f_{RHA}) modules. Instead of recomputing the entire attention mechanism, the RB directly reuses the attention components ($A_{map}^{(a)}$, $A_{qk}^{(a)}$) pre calculated by the corresponding a th module in the SB as

$$F'_{2,a+1} = f_{RHA}^{(a)}(F'_{2,a}, A_{map}^{(a)}, A_{qk}^{(a)}) \quad (5)$$

The architecture concludes with the same LKD and ESA layers as the SB to produce the final output, F_{out} . This semi sharing strategy allows the BERFG to maintain the powerful feature representation of deep attention while substantially lowering the computational burden.

3.4. High performance attention

Prior work [17] has shown that enlarging the receptive field improves information aggregation. Therefore, we propose an HPA module to optimize the learned information described as

$$\begin{aligned} F_{mlp} &= f_{\text{ConvMLP}}(f_{\text{LN}}(\mathbf{X})) \\ F_1 &= f_{\text{FWA}}(f_{\text{LN}}(F_{mlp})) \end{aligned} \quad (6)$$

with LN being the normalization and Convolutional layer, ConvMLP being the Multi layer Perceptron with the kernel size of seven, and Flash Attention is for the Large Window Attention. We first apply ConvMLP to capture local context without relying on explicit QKV projections. To efficiently aggregate information over a larger spatial area, we incorporate Window Attention with a 32×32 window size. However, standard self attention over large windows is computationally expensive due to its quadratic memory and runtime complexity. To address this, we adopt Flash Attention, which enables exact attention computation with significantly lower memory usage and faster execution, making large window self attention feasible. Nevertheless, the effective receptive field remains constrained. To overcome this, we introduce a hybrid module, as detailed below.

3.5. Shared and Receive Hybrid Attention

The core concept of our work is to expand the model effective receptive field while maintaining a balance between high performance and a lightweight design. To achieve this, we propose a solution with two main pillars. First, we introduce a semi sharing mechanism that dramatically reduces computational overhead without sacrificing representational power. Second, we design a Hybrid Attention Module that captures local, global, and channel information effectively. Together, these two innovations allow our model to capture more of the information while staying fast and efficient. The detail of the architecture is shown in Fig. 3.

Semi sharing mechanism. To achieve a lightweight yet high performance design, we introduce a semi sharing mechanism across Hybrid Attention (HA) Module pairs. As illustrated in Fig. 3a, SHA consists of Shared Window Multi Head Attention (Shared WMHA) and Shared Dual Fusion Layer (SDFL), while RHA is composed of Received Window Multi Head Attention (Received WMHA) and Dual Fusion Receiver Layer (DFRL). In this design, the attention map from Shared WMHA is shared with Received WMHA, reducing redundant computation. Unlike standard Softmax attention, which derives the map as $\text{Softmax}(\mathbf{Q}\mathbf{K}^T)$, the Dual Fusion Layer computes it as $\phi(\mathbf{Q})\phi(\mathbf{K})^T$. Within this layer, dynamic feature maps with \mathbf{Q} and \mathbf{K} are recomputed independently at each layer. This dynamic recomputation refreshes feature representations while maintaining efficiency. Overall, the semi sharing mechanism balances representation renewal and computational cost, a trade off validated by our ablation studies.

Local spatial module. Following previous study [18], we employ window based multi head self attention (WMSA) to extract fine local textures (Fig. 3). This design emphasizes the immediate neighborhood of each pixel, allowing high fidelity local restoration.

Global and channel modules. The goal of our dual fusion layer is to efficiently aggregate global spatial and channel information. First, $\mathbf{Q}, \mathbf{K}, \mathbf{V} \in \mathbb{R}^{HW \times C/2}$ are computed over the input token $\mathbf{X} \in \mathbb{R}^{HW \times C}$ according to

$$\mathbf{Q} = \mathbf{W}_Q \mathbf{X}; \quad \mathbf{K} = \mathbf{W}_K \mathbf{X}; \quad \mathbf{V} = \mathbf{W}_V \mathbf{X}; \quad (7)$$

where $\mathbf{W}_Q, \mathbf{W}_K$, and \mathbf{W}_V are projection matrices. To reduce redundancy and computation, we project from dimension C to $C/2$, which halves the feature channels and lightens the model without sacrificing critical information. The tensors are then fed into the spatial, global, and channel branches.

For the spatial branch, we introduce Hedgehog attention (HgA) depicted in Fig. 3b. We also integrate a lightweight depthwise convolution into the computation process, which can be formulated as

$$F_{sb} = (\phi(\mathbf{Q}))(\phi(\mathbf{K}))^T \mathbf{V} + \mathbf{W}_d \mathbf{V}, \quad (8)$$

where \mathbf{W}_d denotes a depthwise convolution and ϕ is the HFM. We denote the spatial branch output as F_{sp} . The HFM learns multi scale feature interactions and enhances the model ability to capture complex spatial dependencies. In addition, we use Fourier Feature Map [11] to boost spatial attention performance by informing the pixel relative position in image. A depthwise convolution is included to capture local structure and complement global attention.

For the channel branch, the self attention mechanism in the CA mechanism is performed along the channel dimension as depicted in Fig. 3c. Following prior channel attention designs, we compute channel wise attention as

$$F_{cb} = \text{softmax}(\mathbf{Q}^T \mathbf{K}) \mathbf{V}, \quad (9)$$

where F_{cb} is the output of channel branch.

Finally, F_{sb} and F_{cb} are concatenated to get the final output. In terms of computational complexity, both the global spatial branch and the channel branch have linear complexity in spatial resolution. To be more specific, the number of multiply add operations required by both the global spatial branch and the channel branch is

$$\mathcal{O}_{\text{DFL}} = \underbrace{2C^2 HW}_{\text{channel branch}} + \underbrace{\left(6 HW \frac{C^2}{D} + 9 HW C\right)}_{\text{spatial branch}}. \quad (10)$$

where D denotes the number of heads and the complexity of the channel branch is written in blue and the spatial branch is written in red. This shows that our dual fusion layer achieves *linear complexity* in spatial resolution while still maintaining high efficiency.

3.6. Large Kernel Distillation

To further refine features with a focus on a wide range of spatial dependencies, we incorporate a Large Kernel Distillation module (Fig. 3d). We distill computation onto the most informative channels while preserving full content through a lightweight bypass. We split channels into a fine grained subset $\mathbf{F}_{fg} \in \mathbb{R}^{H \times W \times C_{fg}}$ and a coarse subset $\mathbf{F}_{cg} \in \mathbb{R}^{H \times W \times (C - C_{fg})}$ with $C_{fg} = \max(C/4, 16)$

$$\mathbf{F}_{fg}, \mathbf{F}_{cg} = \text{Split}(\mathbf{X}), \quad \mathbf{F}_{b+1} = \text{Concat}(f_{\text{TFE}}(\mathbf{F}_{fg}), \mathbf{F}_{cg}). \quad (11)$$

The Triple Feature Extraction (TFE) module consists of three parallel branches. A *channel attention branch* extracts channel information, a *local branch* with a $1 \times 1 \rightarrow 3 \times 3 \rightarrow 1 \times 1$ bottleneck captures fine grained details, and a *hierarchical large kernel branch* uses depthwise and dilated separable convolutions to model long range context. This design achieves high efficiency by restricting heavy computation to C_{fg} channels, which proportionally reduces computation. Simultaneously, the large kernel path efficiently expands the receptive field using dilation and depthwise factorization. Full architectural details, complexity, and effective receptive field analysis are in the supplementary material.

4. Experiments

To validate our proposed UCAN models, this section presents its performance on SR task. The evaluation was conducted across five different test sets. We will describe the methodologies and datasets used in our experiments and present a series of ablation studies to confirm the significance of each proposed module.

4.1. Classic image super-resolution

For evaluating our proposed architectures on traditional super-resolution tasks, we utilized five standard benchmark datasets (Set5 [2], Set14 [37], BSDS100 [24], Urban100 [12], Manga109 [25]) and assessed performance using PSNR and SSIM metrics calculated on the luminance channel following border cropping based on scaling factors and YCbCr color space conversion. Performance analysis involved reconstructing HD images (1280×720), while computational efficiency was measured using multiply-accumulate operations (MACs) via the fvc core library. We present two model variants: UCAN, designed for parameter efficiency, and UCAN-L, optimized for maximizing PSNR and SSIM performance.

4.2. Training Configuration

Our model is trained using a batch size of 16, with input images randomly cropped to 64×64 pixels and augmented through random rotation and horizontal flipping operations. The optimization employs the Adam optimizer ($\beta_1 = 0.9$, $\beta_2 = 0.99$) to minimize L1 reconstruction loss, LDL loss

[19] and Wavelet loss [15], following established super-resolution practices. For $\times 2$ scale factor, we train from scratch for 800,000 iterations with an initial learning rate of 5×10^{-4} , applying step-wise decay by half at milestones [300K, 500K, 650K, 700K, 750K]. Higher magnification factors ($\times 3$ and $\times 4$) utilize transfer learning by fine-tuning the pre-trained $\times 2$ model for 400,000 iterations, maintaining the same initial learning rate with decay at [200K, 320K, 360K, 380K] iterations. All experiments are implemented in PyTorch on 2 RTX 3090 GPUs.

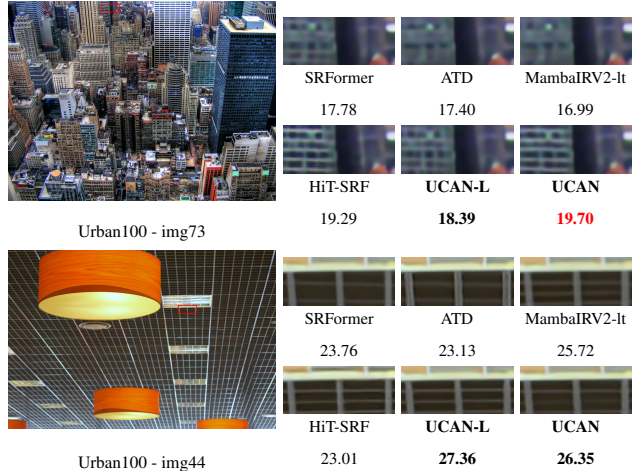


Figure 4. Visual comparison between ground truth and different methods on Urban100.

4.3. Benchmarking with State-of-the-Art Approaches

In this section, we evaluate the effectiveness of our UCAN, UCAN-L model by comparing it with state-of-the-art (SOTA) methods, including CNN-based, lightweight Transformer-based, and SSM-based super-resolution (SR) approaches. We present both quantitative and qualitative results, highlighting comparisons with previous SR models such as SwinIR-light [18], ELAN [40], OmniSR [33], SRformer-light [44], ATD-light [38], HiT-SRF [41], ASID-D8 [26], MambaIR-light[10], MambaIRV2-light [8], RDN [43], RCAN[42] and ESC.

We present a comprehensive comparison of our models against prior state-of-the-art lightweight SR methods, with visual results in Fig. 4 and quantitative metrics in Table 1.

Our base model, UCAN, demonstrates exceptional efficiency. For instance, on the Manga109 ($\times 4$) dataset, it achieves a significant 0.26 dB PSNR improvement over MambaIRV2 while requiring 11% fewer parameters. Similarly, when compared to ASID-D8, UCAN delivers superior performance across the evaluation sets despite having 6% fewer parameters and 23% lower MACs.

The larger variant, UCAN-L, further solidifies our lead. Despite having 7% fewer parameters than the strong ESC

Table 1. Quantitative comparison on *lightweight image super-resolution* with state-of-the-art methods. The best and second-best results are shown in **bold** and underlined, respectively.

Method	scale	#param	MACs	Set5		Set14		BSDS100		Urban100		Manga109	
				PSNR	SSIM								
MambaIR-light [10]	2×	905K	334.2G	38.13	0.9610	33.95	0.9208	32.31	0.9013	32.85	0.9349	39.20	0.9782
OmniSR [33]	2×	772K	194.5G	38.22	0.9613	33.98	0.9210	32.36	0.9020	33.05	0.9363	39.28	0.9784
SRFormer-light [44]	2×	853K	236.3G	38.23	0.9613	33.94	0.9209	32.36	0.9019	32.91	0.9353	39.28	0.9785
ATD-light [38]	2×	753K	380.0G	38.29	0.9616	34.10	0.9217	32.39	0.9023	33.27	0.9375	39.52	0.9789
HiT-SRF [41]	2×	847K	226.5G	38.26	0.9615	34.01	0.9214	32.37	0.9023	33.13	0.9372	39.47	0.9787
ASID-D8 [26]	2×	732K	190.5G [†]	38.32	<u>0.9618</u>	<u>34.24</u>	<u>0.9232</u>	32.40	<u>0.9028</u>	33.35	<u>0.9387</u>	-	-
MambaRV2-light [9]	2×	774K	286.3G	38.26	0.9615	34.09	0.9221	32.36	0.9019	33.26	0.9378	39.35	0.9785
RDN [43]	2×	22123K	5096.2G	38.24	0.9614	34.01	0.9212	32.34	0.9017	32.89	0.9353	39.18	0.9780
RCAN [42]	2×	15445K	3529.7G	38.27	0.9614	34.12	0.9216	<u>32.41</u>	0.9027	33.34	0.9384	39.44	0.9786
ESC [26]	2×	947K	592.0G	<u>38.35</u>	0.9619	34.11	0.9223	<u>32.41</u>	0.9027	33.46	0.9395	<u>39.54</u>	0.9790
UCAN (Our)	2×	689K	146.3G	38.34	<u>0.9618</u>	34.27	0.9242	32.39	0.9025	33.22	0.9379	<u>39.54</u>	0.9790
UCAN-L (Our)	2×	886K	182.4G	38.37	0.9619	34.19	0.9224	32.44	0.9031	<u>33.39</u>	<u>0.9393</u>	39.66	<u>0.9789</u>
MambaIR-light [10]	3×	913K	148.5G	34.63	0.9288	30.54	0.8459	29.23	0.8084	28.70	0.8631	34.12	0.9479
OmniSR [33]	3×	780K	88.4G	34.70	0.9294	30.57	0.8469	29.28	0.8094	28.84	0.8656	34.22	0.9487
SRFormer-light [44]	3×	861K	105.4G	34.67	0.9296	30.57	0.8469	29.26	0.8099	28.81	0.8655	34.19	0.9489
ATD-light [38]	3×	760K	168.0G	34.74	0.9300	30.68	0.8485	<u>29.32</u>	0.8109	<u>29.17</u>	0.8709	34.60	0.9506
HiT-SRF [41]	3×	855K	101.6G	34.75	0.9300	30.61	0.8475	29.29	0.8106	28.99	0.8687	34.53	0.9502
ASID-D8 [26]	3×	739K	86.4G	34.84	0.9307	30.66	0.8491	<u>29.32</u>	<u>0.8119</u>	29.08	0.8706	-	-
MambaRV2-light [9]	3×	781K	126.7G	34.71	0.9298	30.68	0.8483	29.26	0.8098	29.01	0.8689	34.41	0.9497
RDN [43]	3×	22308K	2281.2G	34.71	0.9296	30.57	0.8468	29.26	0.8093	28.80	0.8653	34.13	0.9484
RCAN [42]	3×	15629K	1586.1G	34.74	0.9299	30.65	0.8482	<u>29.32</u>	0.8111	29.09	0.8702	34.44	0.9499
ESC [26]	3×	955K	267.6G	34.84	<u>0.9308</u>	<u>30.74</u>	<u>0.8493</u>	29.34	0.8118	<u>29.28</u>	0.8739	<u>34.66</u>	<u>0.9512</u>
UCAN (Our)	3×	696K	64.6G	<u>34.83</u>	<u>0.9308</u>	30.72	0.8493	<u>29.32</u>	<u>0.8121</u>	29.15	0.8712	34.62	0.9508
UCAN-L(Our)	3×	893K	81.3G	34.81	0.9311	30.75	0.8500	29.34	0.8127	29.29	<u>0.8738</u>	34.79	0.9516
MambaIR-light [10]	4×	924K	84.6G	32.42	0.8977	28.74	0.7847	27.68	0.7400	26.52	0.7983	30.94	0.9135
OmniSR [33]	4×	792K	50.9G	32.49	0.8988	28.78	0.7859	27.71	0.7415	26.64	0.8018	31.02	0.9151
SRFormer-light [44]	4×	873K	62.8G	32.51	0.8988	28.82	0.7872	27.73	0.7422	26.67	0.8032	31.17	0.9165
ATD-light [38]	4×	769K	100.1G	32.63	0.8998	28.89	0.7886	<u>27.79</u>	0.7440	<u>26.97</u>	0.8107	31.48	0.9198
HiT-SRF [41]	4×	866K	58.0G	32.55	0.8999	28.87	0.7880	27.75	0.7432	26.80	0.8069	31.26	0.9171
ASID-D8 [26]	4×	748K	49.6G	32.57	0.8990	28.89	0.7898	27.78	0.7449	26.89	0.8096	-	-
MambaRV2-light [9]	4×	790K	75.6G	32.51	0.8992	28.84	0.7878	27.75	0.7426	26.82	0.8079	31.24	0.9182
RDN [43]	4×	22271K	1309.2G	32.47	0.8990	28.81	0.7871	27.72	0.7419	26.61	0.8028	31.00	0.9151
RCAN [42]	4×	15592K	917.6G	<u>32.63</u>	0.9002	28.87	0.7889	27.77	0.7436	26.82	0.8087	31.22	0.9173
ESC [26]	4×	968K	149.2G	32.68	<u>0.9011</u>	<u>28.93</u>	<u>0.7902</u>	27.80	<u>0.7447</u>	27.07	0.8144	<u>31.54</u>	<u>0.9207</u>
UCAN (Our)	4×	705K	38.1G	<u>32.65</u>	0.9010	<u>28.95</u>	0.7899	<u>27.79</u>	<u>0.7454</u>	26.89	0.8097	<u>31.50</u>	0.9200
UCAN-L (Our)	4×	902K	48.4G	32.68	0.9015	28.99	0.7917	27.80	0.7459	<u>27.06</u>	<u>0.8134</u>	31.63	0.9212

model, UCAN-L outperforms it on four out of the five benchmark datasets. This is particularly evident on Manga109 ($\times 2$), where our model achieves a notable gain of nearly 0.1 dB. These results collectively underscore UCAN’s design as a robust, powerful, and resource-efficient solution for modern image super-resolution.

4.4. Efficient Receptive Field Comparison

We present a comprehensive ERF analysis in Fig. 5, comparing our proposed UCAN model with other models that exploit global spatial information. The ERF images show that UCAN exhibits significantly darker and more extended regions of influence than existing methods. This improved receptive field coverage indicates that our model effectively captures broader contextual information from the input, leading to superior feature representation and ultimately achieving better image reconstruction performance.

4.5. Local Attribution Maps

To assess the information aggregation performance of UCAN, we utilize Local Attribution Maps (LAM) [7]. LAM is a technique designed to identify which pixels in an input

image most strongly influence the final SR output. These regions are known as informative areas, and their size corresponds to the ability of the model to aggregate information. As illustrated in Fig. 6, we applied the LAM method to SRFormer [44], ATD [38], HiT-SRF [41] and UCAN to compare their respective informative areas for identical target regions. SRFormer operates with small, fixed windows that produce locally confined informative areas, thereby limiting its ability to capture long-range dependencies. While ATD and UCAN have expanded these information domains through global attention mechanisms, our model demon-

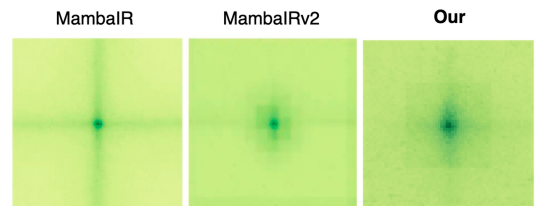


Figure 5. Visualize in detail ERF of MambaIR [10], MambaRV2[8] and UCAN

strates superior information aggregation capabilities. Consequently, our method can leverage information from significantly broader contexts, including repetitive patterns and similar structures across the image, leading to enhanced super-resolution performance.

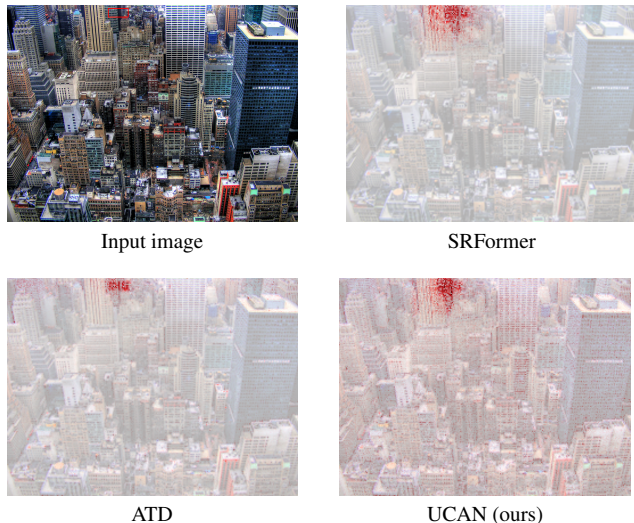


Figure 6. Local attribution maps (LAM) comparison of different super-resolution methods at scale $\times 4$.

4.6. Performance analysis on Attention schemes

Table 2. Comparison of Latency and Parameters between Naive Self-Attention, Flash Attention [3], and the Dual Fusion Layer (DFL)

Module	$\mathbb{R}^{64 \times 64 \times 64}$		$\mathbb{R}^{128 \times 128 \times 64}$	
	Latency (ms)	#params	Latency (ms)	#params
Attention	596.53 (1.5 \times)	0.033M	2576.75 (1.0 \times)	0.082M
Flash Attention	190.50 (4.7 \times)		191.80 (13.4 \times)	
DFL	903.47 (1.0 \times)	0.014M	1294.83 (2.0 \times)	0.014M

Efficient long-range interaction is vital for high-resolution super-resolution, yet conventional self-attention struggles with rapidly increasing memory and latency as resolution grows. UCAN overcomes this limitation by combining Flash Attention, which handles large-window modeling efficiently, with a DLF that aggregates global context at constant complexity. Table 2 presents a comparison of latency and parameter counts for Native Self-Attention, Flash Attention, and DFL measured over 1000 images on an A100 GPU. Flash Attention achieves up to 13.4 \times faster processing than vanilla attention at 128×128 spatial resolution, demonstrating excellent scalability when memory constraints tighten. At smaller resolutions such as 64×64 , the DFL shows slightly higher latency, yet it becomes about twice as fast at larger scales, confirming its efficiency for high-resolution reconstruction. Its parameter count remains stable across resolutions, unlike self-attention whose cost grows with feature dimension,

showing that the hybrid design of UCAN balances local efficiency and global awareness effectively.

4.7. Ablation study

First, we examined the HPA block under two configurations: complete removal and a regular 16×16 window. Both variants led to noticeable performance degradation compared to UCAN, confirming that our default 32×32 setting provides the optimal balance. Next, we compared an 8×8 window with the standard 16×16 configuration in the WMHA block. The smaller window resulted in a substantial performance drop, indicating that further reduction in window size compromises feature aggregation and overall accuracy. We then varied the kernel size (KS) to 5×5 and 47×47 to determine its effect. The 5×5 setting produced a smaller receptive field, limiting contextual awareness, while the 47×47 setting introduced excessive padding that degraded performance. In both cases, due to the distillation-based architecture, we observed a marked drop in accuracy on Urban100, which contains highly detailed textures. Finally, we evaluated the semi-sharing mechanism against full sharing (i.e., parameters computed once and reused across layers). The semi-sharing approach achieved better results, confirming that refreshing new information across layers is essential for maintaining representation diversity.

Table 3. Ablation study. We train all models on DIV2K for 400K iterations, and test on Set5 and Urban100 ($\times 2$). The final result is shown in the last row.

Block	Case	Set5		Urban100	
		PSNR	SSIM	PSNR	SSIM
High performance	w/o HPA	38.27	0.9616	32.90	0.9346
attention (HPA)	window 16×16	38.32	0.9617	33.04	0.9364
WMHA	WS 8×8	38.32	0.9617	33.02	0.9361
Dual Fusion	Using ReLU	38.33	0.9618	33.16	0.9374
Layer (DFL)	Using ELU + 1	38.33	0.9618	33.16	0.9373
Large Kernel	KS = 5×5	38.33	0.9618	33.12	0.9369
Distillation (LKD)	KS = 47×47	38.34	0.9618	33.15	0.9372
Sharing	Sharing Full	38.29	0.9617	32.89	0.9350
UCAN	Our	38.34	0.9618	33.22	0.9379

5. Conclusion

In this paper, we propose UCAN, a novel and lightweight network for image super-resolution that targets the significant memory and computational demands of Transformer-based models. UCAN strategically expands the receptive field with enhanced Flash and Linear Attention, which our experiments show is critical for performance. Furthermore, we introduce an efficient parameter-sharing scheme together with a distillation-based large-kernel convolution module to ensure efficiency. This dual approach reduces computational load while boosting reconstruction quality. As a result, UCAN harnesses Transformer capacity for high-fidelity image reconstruction while remaining lightweight and practical, establishing an effective direction for efficient SR networks

References

- [1] Yuang Ai, Huaibo Huang, Tao Wu, Qihang Fan, and Ran He. Breaking complexity barriers: High-resolution image restoration with rank enhanced linear attention. *arXiv preprint arXiv:2505.16157*, 2025. 2
- [2] Marco Bevilacqua, Aline Roumy, Christine Guillemot, and Marie Line Alberi-Morel. Low-complexity single-image super-resolution based on nonnegative neighbor embedding. 2012. 6
- [3] Tri Dao, Dan Fu, Stefano Ermon, Atri Rudra, and Christopher Ré. Flashattention: Fast and memory-efficient exact attention with io-awareness. *Advances in neural information processing systems*, 35:16344–16359, 2022. 8
- [4] Chao Dong, Chen Change Loy, Kaiming He, and Xiaoou Tang. Learning a deep convolutional network for image super-resolution. In *Computer Vision–ECCV 2014: 13th European Conference, Zurich, Switzerland, September 6–12, 2014, Proceedings, Part IV 13*, pages 184–199. Springer, 2014. 2
- [5] Chao Dong, Yubin Deng, Chen Change Loy, and Xiaoou Tang. Compression artifacts reduction by a deep convolutional network. In *Proceedings of the IEEE international conference on computer vision*, pages 576–584, 2015. 2
- [6] Alexey Dosovitskiy. An image is worth 16x16 words: Transformers for image recognition at scale. *arXiv preprint arXiv:2010.11929*, 2020. 2
- [7] Jinjin Gu and Chao Dong. Interpreting super-resolution networks with local attribution maps. In *Proceedings of the IEEE/CVF conference on computer vision and pattern recognition*, pages 9199–9208, 2021. 7
- [8] Hang Guo, Yong Guo, Yaohua Zha, Yulun Zhang, Wenbo Li, Tao Dai, Shu-Tao Xia, and Yawei Li. Mambairv2: Attentive state space restoration. *arXiv preprint arXiv:2411.15269*, 2024. 2, 3, 6, 7
- [9] Hang Guo, Yong Guo, Yaohua Zha, Yulun Zhang, Wenbo Li, Tao Dai, Shu-Tao Xia, and Yawei Li. Mambairv2: Attentive state space restoration, 2024. 7
- [10] Hang Guo, Jinmin Li, Tao Dai, Zhihao Ouyang, Xudong Ren, and Shu-Tao Xia. Mambair: A simple baseline for image restoration with state-space model. In *European Conference on Computer Vision*, pages 222–241. Springer, 2025. 6, 7
- [11] Ermo Hua, Che Jiang, Xingtai Lv, Kaiyan Zhang, Youbang Sun, Yuchen Fan, Xuekai Zhu, Biqing Qi, Ning Ding, and Bowen Zhou. Fourier position embedding: Enhancing attention’s periodic extension for length generalization. *arXiv preprint arXiv:2412.17739*, 2024. 5
- [12] Jia-Bin Huang, Abhishek Singh, and Narendra Ahuja. Single image super-resolution from transformed self-exemplars. In *Proceedings of the IEEE conference on computer vision and pattern recognition*, pages 5197–5206, 2015. 6
- [13] Zheng Hui, Xiumei Wang, and Xinbo Gao. Fast and accurate single image super-resolution via information distillation network. In *Proceedings of the IEEE conference on computer vision and pattern recognition*, pages 723–731, 2018. 2
- [14] Jiwon Kim, Jung Kwon Lee, and Kyoung Mu Lee. Deeply-recursive convolutional network for image super-resolution. In *Proceedings of the IEEE conference on computer vision and pattern recognition*, pages 1637–1645, 2016. 2
- [15] Cansu Korkmaz and A Murat Tekalp. Training transformer models by wavelet losses improves quantitative and visual performance in single image super-resolution. In *Proceedings of the IEEE/CVF Conference on Computer Vision and Pattern Recognition*, pages 6661–6670, 2024. 6
- [16] Kin Wai Lau, Lai-Man Po, and Yasar Abbas Ur Rehman. Large separable kernel attention: Rethinking the large kernel attention design in cnn. *Expert Systems with Applications*, 236:121352, 2024. 3
- [17] Dongheon Lee, Seokju Yun, and Youngmin Ro. Emulating self-attention with convolution for efficient image super-resolution. *arXiv preprint arXiv:2503.06671*, 2025. 3, 5
- [18] Jingyun Liang, Jie Zhang Cao, Guolei Sun, Kai Zhang, Luc Van Gool, and Radu Timofte. Swinir: Image restoration using swin transformer. In *Proceedings of the IEEE/CVF international conference on computer vision*, pages 1833–1844, 2021. 5, 6
- [19] Jie Liang, Hui Zeng, and Lei Zhang. Details or artifacts: A locally discriminative learning approach to realistic image super-resolution. In *Proceedings of the IEEE/CVF conference on computer vision and pattern recognition*, pages 5657–5666, 2022. 6
- [20] Bee Lim, Sanghyun Son, Heewon Kim, Seungjun Nah, and Kyoung Mu Lee. Enhanced deep residual networks for single image super-resolution. In *Proceedings of the IEEE conference on computer vision and pattern recognition workshops*, pages 136–144, 2017. 2
- [21] Jie Liu, Wenjie Zhang, Yuting Tang, Jie Tang, and Gangshan Wu. Residual feature aggregation network for image super-resolution. In *Proceedings of the IEEE/CVF conference on computer vision and pattern recognition*, pages 2359–2368, 2020. 4
- [22] Ze Liu, Yutong Lin, Yue Cao, Han Hu, Yixuan Wei, Zheng Zhang, Stephen Lin, and Baining Guo. Swin transformer: Hierarchical vision transformer using shifted windows. In *Proceedings of the IEEE/CVF international conference on computer vision*, pages 10012–10022, 2021. 2
- [23] Zhisheng Lu, Juncheng Li, Hong Liu, Chaoyan Huang, Linlin Zhang, and Tiejiong Zeng. Transformer for single image super-resolution. In *Proceedings of the IEEE/CVF conference on computer vision and pattern recognition*, pages 457–466, 2022. 2
- [24] David Martin, Charless Fowlkes, Doron Tal, and Jitendra Malik. A database of human segmented natural images and its application to evaluating segmentation algorithms and measuring ecological statistics. In *Proceedings eighth IEEE international conference on computer vision. ICCV 2001*, pages 416–423. IEEE, 2001. 6
- [25] Yusuke Matsui, Kota Ito, Yuji Aramaki, Azuma Fujimoto, Toru Ogawa, Toshihiko Yamasaki, and Kiyoharu Aizawa. Sketch-based manga retrieval using manga109 dataset. *Multimedia tools and applications*, 76(20):21811–21838, 2017. 6
- [26] Karam Park, Jae Woong Soh, and Nam Ik Cho. Efficient attention-sharing information distillation transformer for lightweight single image super-resolution. In *Proceedings of the AAAI Conference on Artificial Intelligence*, pages 6416–6424, 2025. 2, 3, 4, 6, 7

- [27] René Ranftl, Alexey Bochkovskiy, and Vladlen Koltun. Vision transformers for dense prediction. In *Proceedings of the IEEE/CVF international conference on computer vision*, pages 12179–12188, 2021. 2
- [28] Wenzhe Shi, Jose Caballero, Ferenc Huszár, Johannes Totz, Andrew P Aitken, Rob Bishop, Daniel Rueckert, and Zehan Wang. Real-time single image and video super-resolution using an efficient sub-pixel convolutional neural network. In *Proceedings of the IEEE conference on computer vision and pattern recognition*, pages 1874–1883, 2016. 3
- [29] Yuan Shi, Bin Xia, Xiaoyu Jin, Xing Wang, Tianyu Zhao, Xin Xia, Xuefeng Xiao, and Wenming Yang. Vmambair: Visual state space model for image restoration. *arXiv preprint arXiv:2403.11423*, 2024. 2
- [30] Long Sun, Jinshan Pan, and Jinhui Tang. Shufflemixer: An efficient convnet for image super-resolution. *Advances in Neural Information Processing Systems*, 35:17314–17326, 2022. 2
- [31] Christian Szegedy, Vincent Vanhoucke, Sergey Ioffe, Jon Shlens, and Zbigniew Wojna. Rethinking the inception architecture for computer vision. In *Proceedings of the IEEE conference on computer vision and pattern recognition*, pages 2818–2826, 2016. 3
- [32] Ying Tai, Jian Yang, and Xiaoming Liu. Image super-resolution via deep recursive residual network. In *Proceedings of the IEEE conference on computer vision and pattern recognition*, pages 3147–3155, 2017. 2
- [33] Hang Wang, Xuanhong Chen, Bingbing Ni, Yutian Liu, and Jinfan Liu. Omni aggregation networks for lightweight image super-resolution. In *Proceedings of the IEEE/CVF Conference on Computer Vision and Pattern Recognition*, pages 22378–22387, 2023. 2, 6, 7
- [34] Gang Wu, Junjun Jiang, Junpeng Jiang, and Xianming Liu. Transforming image super-resolution: a convformer-based efficient approach. *IEEE Transactions on Image Processing*, 2024. 2
- [35] Chengxing Xie, Xiaoming Zhang, Linze Li, Haiteng Meng, Tianlin Zhang, Tianrui Li, and Xiaole Zhao. Large kernel distillation network for efficient single image super-resolution. In *Proceedings of the IEEE/CVF conference on computer vision and pattern recognition*, pages 1283–1292, 2023. 2
- [36] Syed Waqas Zamir, Aditya Arora, Salman Khan, Munawar Hayat, Fahad Shahbaz Khan, and Ming-Hsuan Yang. Restormer: Efficient transformer for high-resolution image restoration. In *Proceedings of the IEEE/CVF conference on computer vision and pattern recognition*, pages 5728–5739, 2022. 2
- [37] Roman Zeyde, Michael Elad, and Matan Protter. On single image scale-up using sparse-representations. In *International conference on curves and surfaces*, pages 711–730. Springer, 2010. 6
- [38] Leheng Zhang, Yawei Li, Xingyu Zhou, Xiaorui Zhao, and Shuhang Gu. Transcending the limit of local window: Advanced super-resolution transformer with adaptive token dictionary. In *Proceedings of the IEEE/CVF conference on computer vision and pattern recognition*, pages 2856–2865, 2024. 2, 3, 6, 7
- [39] Michael Zhang, Kush Bhatia, Hermann Kumbong, and Christopher Ré. The hedgehog & the porcupine: Expressive linear attentions with softmax mimicry. *arXiv preprint arXiv:2402.04347*, 2024. 3
- [40] Xindong Zhang, Hui Zeng, Shi Guo, and Lei Zhang. Efficient long-range attention network for image super-resolution. In *European conference on computer vision*, pages 649–667. Springer, 2022. 2, 6
- [41] Xiang Zhang, Yulun Zhang, and Fisher Yu. Hit-sr: Hierarchical transformer for efficient image super-resolution. In *European Conference on Computer Vision*, pages 483–500. Springer, 2024. 6, 7
- [42] Yulun Zhang, Kunpeng Li, Kai Li, Lichen Wang, Bineng Zhong, and Yun Fu. Image super-resolution using very deep residual channel attention networks. In *Proceedings of the European conference on computer vision (ECCV)*, pages 286–301, 2018. 2, 6, 7
- [43] Yulun Zhang, Yapeng Tian, Yu Kong, Bineng Zhong, and Yun Fu. Residual dense network for image super-resolution. In *Proceedings of the IEEE conference on computer vision and pattern recognition*, pages 2472–2481, 2018. 2, 6, 7
- [44] Yupeng Zhou, Zhen Li, Chun-Le Guo, Song Bai, Ming-Ming Cheng, and Qibin Hou. Srformer: Permuted self-attention for single image super-resolution. In *Proceedings of the IEEE/CVF International Conference on Computer Vision*, pages 12780–12791, 2023. 6, 7